Using geogenic radon potential to assess radon priority area designation, a case study around Castleisland, Co. Kerry, Ireland

Banríon, M. H.; Elío, J.; Crowley, Q. G.

Published in:
Journal of Environmental Radioactivity

DOI (link to publication from Publisher):
10.1016/j.jenvrad.2022.106956

Publication date:
2022

Document Version
Publisher's PDF, also known as Version of record

Journal of Environmental Radioactivity 251-252 (2022) 106956

Contents lists available at ScienceDirect

Journal of Environmental Radioactivity

journal homepage: www.elsevier.com/locate/jenvrad

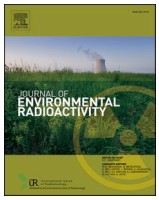

Using geogenic radon potential to assess radon priority area designation, a case study around Castleisland, Co. Kerry, Ireland

M.H. Banríon [a,*], J. Elío [b], Q.G. Crowley [a]

[a] Geology Department, School of Natural Sciences, Trinity College, Dublin 2, Ireland
[b] Department of Planning, Aalborg University Copenhagen, Copenhagen, Denmark

ARTICLE INFO

Keywords:
Radon
Geogenic radon map
Indoor radon
Soil-gas concentrations
Geology

ABSTRACT

Globally, indoor radon exposure is the leading cause of lung cancer in non-smokers and second most common cause after tobacco smoking. Soil-gas radon is the main contributor to indoor radon, but its spatial distribution is highly variable, which poses certain challenges for mapping and predicting radon anomalies. Measurement of indoor radon typically takes place over long periods of time (e.g. 3 months) and is seasonally adjusted to an annual average concentration. In this article we investigate the suitability of using soil-gas radon and soil-permeability measurements for rapid radon risk assessments at local scale. The area of Castleisland, Co. Kerry was chosen as a case study due to availability of indoor radon data and the presence of significant radon anomalies. In total, 135 soil-gas and permeability measurements were collected and complemented with 180 indoor radon measurements for an identical 6 km^2 area. Both soil-gas and indoor radon concentrations ranged from very low (<10 $kBqm^{-3}$, 0.1 Bqm^{-3}) to anomalously high (>1433 $kBqm^{-3}$, 65,000 Bqm^{-3}) values. Our method classifies almost 50% of the area as a high radon potential area, and allows assessment of geogenic controls on radon distribution by including other geological variables. Cumulatively, the percentage of indoor radon variance explained by soil-gas radon concentration, bedrock geology, subsoil permeability and Quaternary geology is 34% (16%, 10%, 4% and 4% respectively). Soil-gas and indoor radon anomalies are associated with black shales, whereas the presence of karst and geological faults are other contributing factors. Sampling of radon soil-gas and soil permeability, used in conjunction with other geogenic data, can therefore facilitate rapid designation of radon priority areas. Such an approach demonstrates the usefulness of high-resolution geogenic maps in predicting indoor radon risk categories when compared to the application of indoor radon measurements alone. This method is particularly useful to assess radon potential in areas where indoor radon measurements are sparse or lacking, with particular application to rural areas, land rezoned for residential use, or for sites prior to building construction.

1. Introduction

The global population receives its most significant proportion of natural ionizing radiation from radon exposure (Monty, 2000). The World Health Organization classifies radon as a class I carcinogen, and reports that it is the second leading cause of lung cancer after tobacco smoking, and the most common cause of lung cancer in non-smokers (World Health Organization, 2009). A study of 66 countries reported 226,057 total radon-attributed lung cancer deaths in 2012 (Gaskin et al., 2018). Annually in Ireland, approximately 350 people are estimated to develop radon-induced lung cancer (Fuente et al., 2020; Murphy et al., 2021). Typical 5-year survival rates from the time of diagnosis for lung cancer are 20% (National Cancer Registry Ireland, 2020). When identified, radon priority area (RPA) can be the focus for radon testing and remediation (Bossew, 2018), or they may be used as a geospatial parameter in targeted lung cancer screening programmes (Elío et al., 2018; Petermann et al., 2022). Any efforts which identify radon priority areas will help to reduce the lung cancer mortality in the general population.

Radon is a naturally occurring radioactive noble gas that emanates from rock, soil, and water. It is a dense, odourless and colourless gas. Radon (^{222}Rn) is an intermediate decay product in the ^{238}U decay chain.

Abbreviations: GRP, Geogenic Radon Potential; IRC, Indoor Radon Concentration; SGRn, Soil-Gas Radon; RPA, Radon Priority Area.

* Corresponding author. Museum Building, Geology department, School of Natural Sciences, Trinity College, Dublin 2, Ireland.
E-mail addresses: mhughes5@tcd.ie (M.H. Banríon), javierdem@plan.aau.dk (J. Elío), crowleyq@tcd.ie (Q.G. Crowley).

https://doi.org/10.1016/j.jenvrad.2022.106956
Received 16 February 2022; Received in revised form 21 June 2022; Accepted 22 June 2022
Available online 30 June 2022

As uranium emits alpha particles, it transforms into a series of different isotopes before decaying to lead (^{206}Pb). The isotopes of ^{219}Rn (actinon) and ^{220}Rn (thoron) are intermediate decay products of ^{235}U and ^{232}Th respectively. Radon concentrations in the atmosphere are generally low (typically 5 becquerels per cubic meter (Bqm^{-3})) (Barros et al., 2015; Gunning, 2016; Habib et al., 2018; Rafique et al., 2021). However, radon can occur at much higher concentrations in soil (typically 10's to 100's kBqm^{-3}) (Abdalla et al., 2021; Alonso et al., 2019), or enclosed spaces such as buildings and caves (typically 10's to 100's Bqm^{-3}) (Cucoş Dinu et al., 2017; Margineanu, 2019; Smith et al., 2019).

As radon decays over a short half-life (3.8 days), it emits alpha radiation (5.5909 MeV) as it transforms into polonium (^{218}Po and ^{214}Po). The short half-life of ^{218}Po and ^{214}Po (164.3μs and 3 min respectively) causes these isotopes to densely emit alpha radiation (energies of 6 MeV and 7.9 MeV respectively). The polonium isotopes, which are charged metal ions, can be inhaled either unattached or attached to airborne particulate matter. The polonium ions can become lodged in lung tissue and act as point sources of alpha radiation. For these reasons, there is a direct relationship between radon exposure and lung cancer (Marsh et al., 2021).

Globally, the detrimental health effects of radon exposure are recognized, and many countries have initiatives designed to mitigate these health issues (European Commission, 2013; Khan et al., 2019; United Nations Scientific Committee on the Effects of Atomic Radiation, 2015). In Ireland, the national radon action plan is supported by the 'National Radon Control Strategy', 'Radon in workplaces', 'Gamma radiation from building materials', and 'Indoor exposure to radon in domestic dwellings' (Radiological Protection Act, 1991; Ionising Radiation Regulations, 2019). Of particular importance is the original radon risk map, which outlines areas of radon priority, with high radon areas defined as "any area where it is predicted that 10 percent or more of homes will exceed the reference level of 200 Becquerel per cubic metre (Bqm^{-3})" (Fennell et al., 2002). In high radon areas, new buildings are obliged to have preventative measures in place to reduce excessive radon accumulation. Furthermore, in areas deemed high radon risk, employers are obliged to measure for radon and if necessary, ensure that radon is below the reference level (Radiological Protection Act, 1991 (Ionizing Radiation) Regulations, 2019). Therefore, finding an effective method for defining high radon areas is crucial for radon mitigation (Bossew et al., 2020).

The original radon risk map of Ireland published by the Environmental Protection Agency (Fennell et al., 2002) has a 10 × 10 km^2 spatial resolution and is based exclusively on indoor radon concentration (IRC) (i.e. it does not contain any geological information). The Environmental Protection Agency in Ireland published an updated radon risk map in May 2022, which incorporates geogenic properties following the methodologies of Elío et al. (2017), (Environmental Protection Agency, 2022). Importantly, the literature on radon and geology indicates a high spatial variability of soil-gas radon (SGRn), over areas far smaller than 10 × 10 km^2 (Duggal et al., 2014, Idriss et al., 2014; Ravikumar et al., 2015).

It is noteworthy that the greatest contributor to IRC is SGRn (Chen and Ford, 2017; World Health Organization, 2007). Porosity, soil permeability, structural geology and the pressure difference between the ground below the building and the indoor ground level, influences SGRn concentrations (Sun et al., 2004; Jelle 2012; Kulali et al., 2017; Laiolo et al., 2016). Both occupancy style, ventilation and building characteristics affect the radon concentrations within dwellings (Liping et al., 2016; Schubert et al., 2018). Additionally, the climatic and seasonal conditions affect the atmospheric pressure, wind speed, temperature, humidity and precipitation, which influence soil-gas radon accumulating indoors (Sundal et al., 2008; Xie et al., 2015).

Ireland's National Radon Control Strategy targets geographical regions deemed to be radon prone, i.e. High Radon Areas (HRA) or Radon Priority Areas (RPA). The National Radon Control Strategy second phase knowledge gaps report states that the national radon risk map may be improved by researching areas with anomalously high radon levels associated with kartsified limestones particularly around Castleisland and Tralee in North Co. Kerry (National Radon Control Strategy, 2019). A specific area in Ireland was chosen as the focus of this study due to anomalous radon reported in the region, and the fact that it is underlain by karstified limestones. The study area is approximately 6 km^2 containing multiple geological units at a 1:100 K scale.

In this paper, the method of geogenic radon potential (GRP); a two-parameter method using SGRn and soil permeability measurements (Neznal et al., 2004), is assessed for suitability to identify radon-prone areas. Results are compared with the original radon map for Ireland (Fennell et al., 2002) and the updated EPA radon map of Ireland (Environmental Protection Agency, 2022). The approach for radon priority area assessment investigated in this study was tested for the townland of Castleisland, Co. Kerry, South-West Ireland (Fig. 1). This area was chosen considering one of Europe's highest, and Ireland's highest IRC measurement of 65,000 Bqm^{-3} was recorded here (seasonally adjusted average of multiple measurements of 49,000 Bqm^{-3}; Organo et al., 2004). Furthermore, the highest underground radon concentrations in Ireland were recorded in Crag Cave, Castleisland (11,285 Bqm^{-3}), during a reconnaissance survey of radon in three show caves in Ireland (Duffy et al., 1996). Approximately half of the study site is classified as a high indoor radon area (Fig. 1) (Environmental Protection Agency, 2022; Fennell et al., 2002).

The main aims of this study are to investigate the use of GRP as a means to assess radon risk and to compare the resultant risk maps with the original map which relies solely on IRC data (Fig. 1) and with the new EPA indoor radon map, which incorporates geological parameters (Environmental Protection Agency, 2022). The data analysis presented here illustrates strong evidence for the GRP method being a suitable process for estimating radon risk in this area. We present results that demonstrate a high spatial variability of radon and that a locally occurring lithology is a major contributor to the high IRC measurements in the Castleisland area. We suggest that radon gas utilizes faults and karst, and is transported from source to areas underlain by limestones. The scientific approach described in this study validates the feasibility for using geogenic data when assessing and defining radon priority areas, especially at local scales and in rural regions with a low population density and limited availability of indoor radon data.

2. Materials and methods

2.1. Study area

Upper Palaeozoic rocks form the bedrock geology of the Castleisland area (www.gsi.ie; Pracht, 1997). The primary bedrock type comprises various Dinantian (359 Ma – 326 Ma) limestones (un-bedded, bedded, bioclastic, argillaceous). The limestones formed in an open water sub-tidal zone on the continental shelf (Sleeman et al., 2004). The north of the study area is dominated by carboniferous siltstones (Cloone Flagstones) and Namurian (326 Ma – 313 Ma) Clare Shales (Pracht, 1997).

The shales accumulated in deep basins which formed after faulting caused by the Variscan orogeny (Sleeman et al., 2004). The Clare Shales are black shales, formed in a deep water euxinic paleoenvironment 326 Ma to 313 Ma overlying Viséan (346.7 Ma to 330.9 Ma) limestones (Hodson, 1954; Rider, 1974; Wignall and Best, 2000). Substantial concentrations (mean 10's to 100's mg kg) of uranium are frequently reported to be contained within black shales (Lecomte et al., 2017; Soesoo et al., 2020). Elevated levels of uranium in organic rich black shales can be attributed to abiotic sequestering or symbiotic remediation processes, i.e. bacteria utilizing uranium for their growth while converting the mobile U(VI) to the immobile U(IV) (Anderson et al., 2003; Gadd, 2010; Koribanics et al., 2015; Min et al., 2005). In abiotic terms, uranium occurs in elevated concentrations in uranyl tricarbonate form, while anoxic conditions cause the uranium to present in higher concentrations

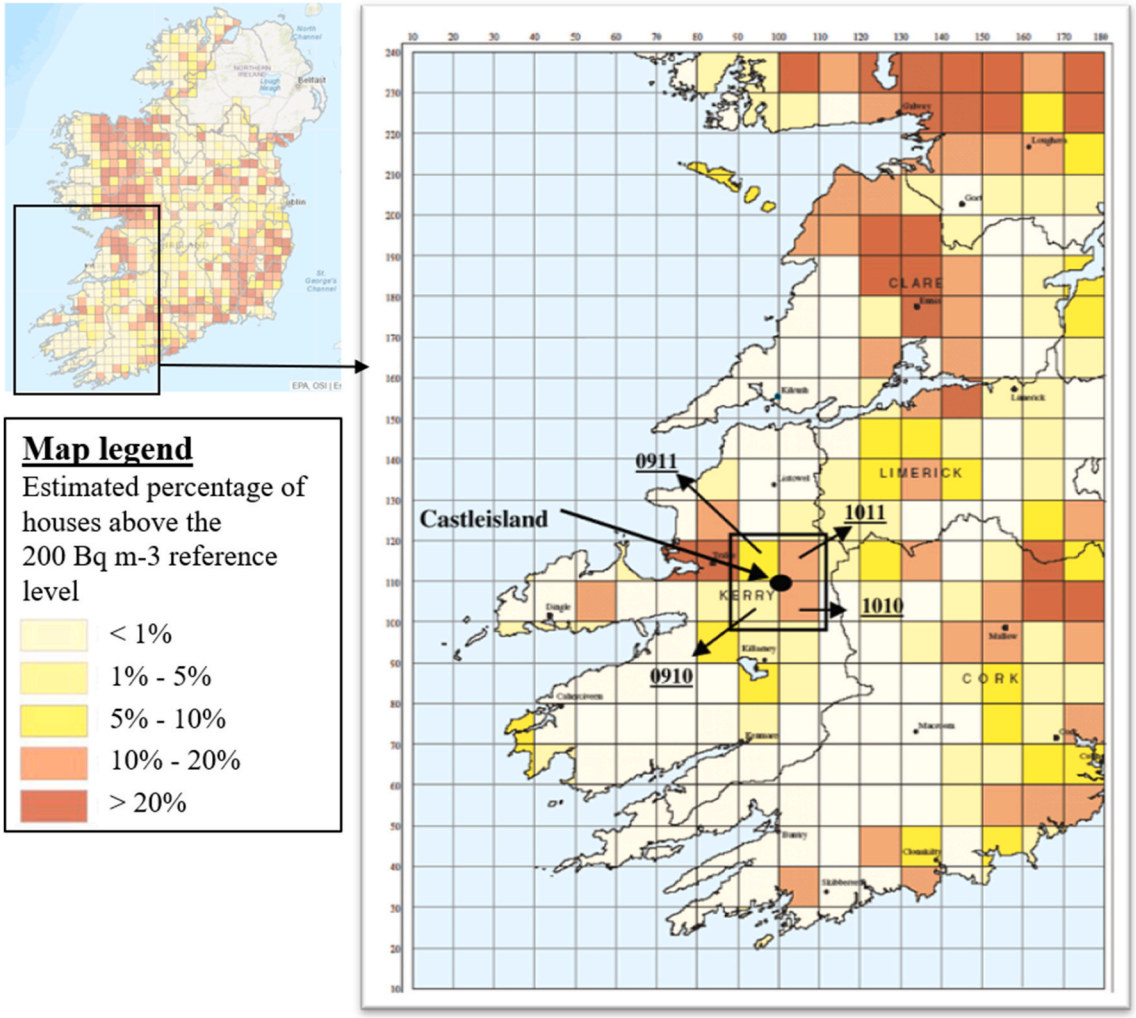

Fig. 1. Top left shows the Indoor radon map for Ireland (Fennell et al., 2002). The right map is adapted from (Organo and Murphy, 2007) which pinpoints the location of the Castleisland study area with consideration to Ireland's radon map. The grids are 10 × 10 km^2. The map legend shows the estimated percentage of homes likely to exceed the 200 Bqm^{-3} reference level.

as uranyl carbonate species, which allows for dissolved U(VI) to precipitate as U(IV) (Nagarajan et al., 2007; Hyun et al., 2014). It is important to note that not all shales are formed in anoxic environments, and that shales inherently vary in their uranium concentration.

Geologically, Castleisland is located at, what is conventionally considered, the northern edge of the Variscan orogeny in Ireland, which caused large-amplitude folds during the late Carboniferous and early Permian periods (Sleeman et al., 2004). Primary structural features of the study area resulted from the Variscan orogeny (Pracht, 1997; Thornton, 1966), including an east-west anticlinal axial plane approximately 1 km to the south. The main faults are directed NS and NW-SE (Fig. 3). The limestone is extensively karstified, exhibiting sinkholes, springs and dolines (www.gsi.ie) and resulting in caves spanning 100's m^2 (Gunn, 1982). Streams in Crag cave (200 m east of the study area) have a north to south flow direction (Tooth and Fairchild, 2003).

Quaternary glaciations affected the area resulting in predominantly locally derived glacial till (Sleeman et al., 2004). Quaternary sediments consist of till derived from Namurian sandstones, siltstones, and shales in the north of the area and till derived from limestones in the south, with alluvium also present in the south.

The exact location of the study area was decided utilizing available information on regional geology (www.gsi.ie). Fig. 2 depicts the study area sampling grid superimposed on geological maps for the area. The grid acted as an aid to collect samples in an equal spatial pattern as much as possible (Fig. 2). In some scenarios it was not possible to collect data at certain locations due to a variety of reasons including the depth to bedrock being too shallow, or where the subsoil was too impermeable to obtain a measurement for GRP calculation. Furthermore, samples were not collected on artificial land (e.g. landscaped gardens). For these reasons, there are a lack of samples on the south-east of the map (Fig. 2) which correlates with the townland of Castleisland Co. Kerry.

2.2. Subsoil permeability measurements

Subsoil permeability measurements were collected using a Radon-Jok device which forms part of the well-established, standardized method (Neznal et al., 2004). A 1-m hollow tube, with a 'lost tip' attached to the bottom, was hammered vertically into the soil, and the tip was ejected at 80 cm to permit the extraction of a soil-gas sample. The hollow tube was connected to the Radon-Jok device using a rubber tube. The Radon-Jok device was activated, and the time to extract 2-L of air from the subsoil was recorded. In cases of lower permeability, one or two weights were attached to the Radon-Jok device in order to reduce the amount of time taken to extract an air sample from the subsurface. The theory of calculating permeability using the Radon-Jok instrument is derived from Darcy's equation:

$$Q = F.\,(k\mu).\,\Delta p, \text{ rearranged as } k = (Q.\,\mu)/(F.\,\Delta p) \quad (1)$$

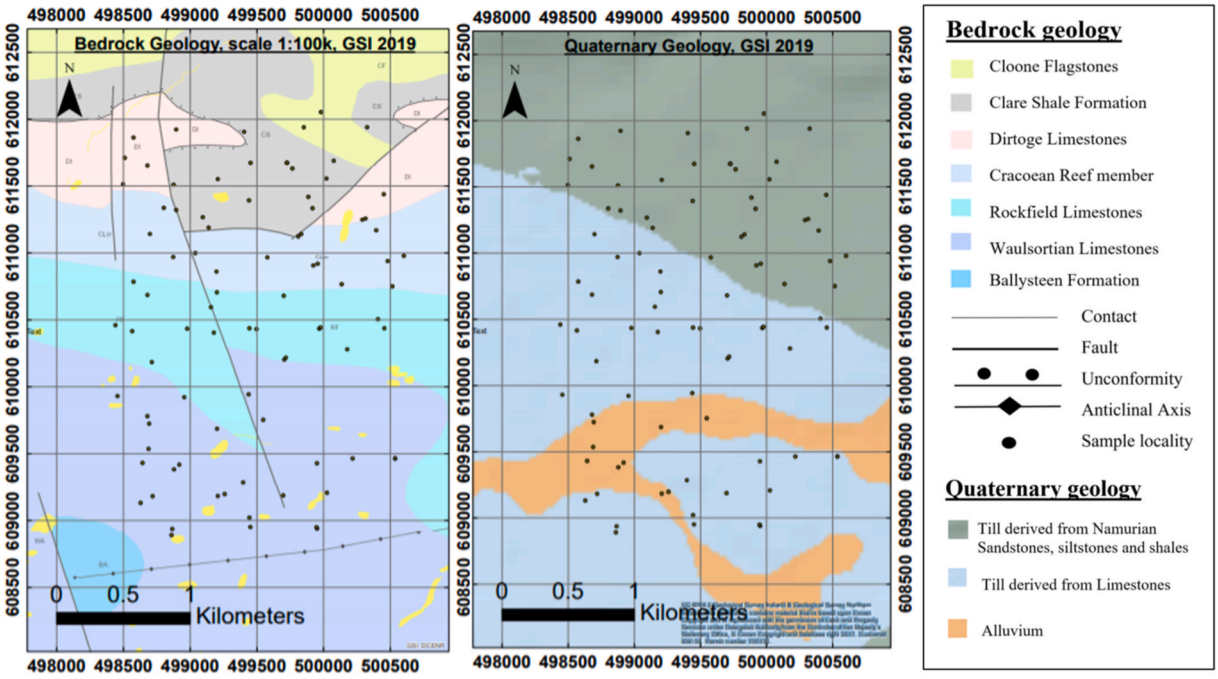

Fig. 2. Illustration of how the sample area was chosen to include a range of geogenic features. The coordinate system used is the Irish Time Mercator (ITM). (a) Bedrock geology 1:100 k scale G.S.I. 2019. (b) Quaternary geology map 1:50 k G.S.I. The points on each map represent the data sample collection locations. The small text at the bottom right side of the Quaternary map reads "CC-BY 4.0 Geological Survey Ireland & Geological Survey Northern Ireland. This publication contains material that is based upon Crown Copyright and is reproduced with the permission of Land and Property Services under Delegated Authority from the Controller of Her Majesty's Stationary Office, © Crown Copyright and database right 2017. Customer ID4104. Permit number 100132.".

Where: k is the permeability (in m^2), F is the shape factor (0.159 m for Radon-Jok), Q is the flow rate (m^3/s Δp is the pressure difference (Pa), and μ is the dynamic viscosity of air (1.75 × 10-5 Pa s @ 10C). Q is calculated from the time taken to fill the 2-L volume of the diaphragm. The pressure is provided by none, one or two weights, applying a pressure of 0, 2160 or 3750 Pa, respectively (Neznal et al., 2004).

2.3. Soil-gas measurements

In total, 135 SGRn samples were collected, including duplicate samples. Ninety-five of these were collected between the July 14, – July 22, 2018. The remaining 40 samples were collected between July 30, – August 2, 2019. In 2019, four samples were collected from control points over the collection period. In 2018, a total of 12 samples were collected from control points over the collection period. These duplicate samples were taken to assess any change in measurement due to atmospheric variability or daily weather fluctuations. In the 2018 field survey, 23 extra samples were collected in the north of the field study, due to a significant radon anomaly. Eight samples were incomplete due to either failure in obtaining permeability readings or soil-gas to sample. These additional, failed and control samples were removed from the dataset for geostatistical analysis to avoid biasing of results. The data analysis included 88 samples in total.

Soil gas was extracted and soil radon concentrations were measured following the procedure of (Neznal et al., 2004). The same hollow tube set-up was used for the subsoil permeability samples to measure the SGRn. A 150 ml syringe was attached to the hollow tube to extract the soil-gas sample. The first two 150 ml samples were discarded to purge the pipe of any atmospheric air. The third sample was transferred into a 250 ml pre-vacuumed ionization chamber. The chamber pressure was equalised to the atmospheric pressure by introducing 100 ml of atmospheric air (atmospheric air contains negligible radon concentrations, typically less than 10 Bqm^{-3}) (Gunning, 2016). Variables of moisture content and particulate matter were mitigated by attaching an interface with a desiccant compartment (containing anhydrous calcium sulphate) and a 0.45 μm filter between the hollow tube and syringe. An RM-2 device was used to measure radon concentration within the soil-gas, 15 min after the sample was introduced into the chamber.

The lower and upper detection limit of the RM-2 device is 3 $kBqm^{-3}$ and 1400 $kBqm^{-3}$, respectively. The radon concentration uncertainty is represented by sigma(σ), where sigma (σ) is 0.33 x(concentration of radon ($kBqm^{-3}$))$^{0.5}$, which results in the radon concentration being reported as concentration of radon±sigma. Therefore, the RM-2 device has a radon concentration measurement uncertainty of less than 20%. Elío et al. (2019) reported an average relative standard deviation of 15% for replicate samples and an average 5.75% uncertainty for the same RM-2 device.

2.4. Geogenic radon potential calculation

We used the geogenic radon potential G(RP) index as defined by (Neznal et al., 2004). The equation for which is:

$$GRP = CRn / (-\log10\,(k) - 10) \quad (2)$$

Where k (m^2) is the soil permeability and CRn is the concentration of radon ($kBqm^{-3}$) in the soil-gas. This method uses both SGRn concentrations ($kBqm^{-3}$) and subsoil permeability measurements (m^2) and outputs a value representing GRP. The calculated GRP is conventionally reported without a unit because it is a categorical and relative value which represents the potential of radon gas entering a building. In order to facilitate comparison with other countries, GRP categories were chosen to reflect those most commonly used, which are 0–10, 10–35 and 35+, corresponding to low, medium and high values respectively. The GRP method as originally defined (Neznal et al., 2004) utilizes at least 15 for a site less or equal to 800 m^2, otherwise individual SGRn and k samples are collected in a 10 × 10 m grid for a specific location (e.g. the area corresponding to a new building). The general GRP method of Neznal et al. (2004) has been adapted for different applications, for instance some studies in Germany use two measurements within a given sample site (Kemski et al., 1996), in other studies there is one sample per

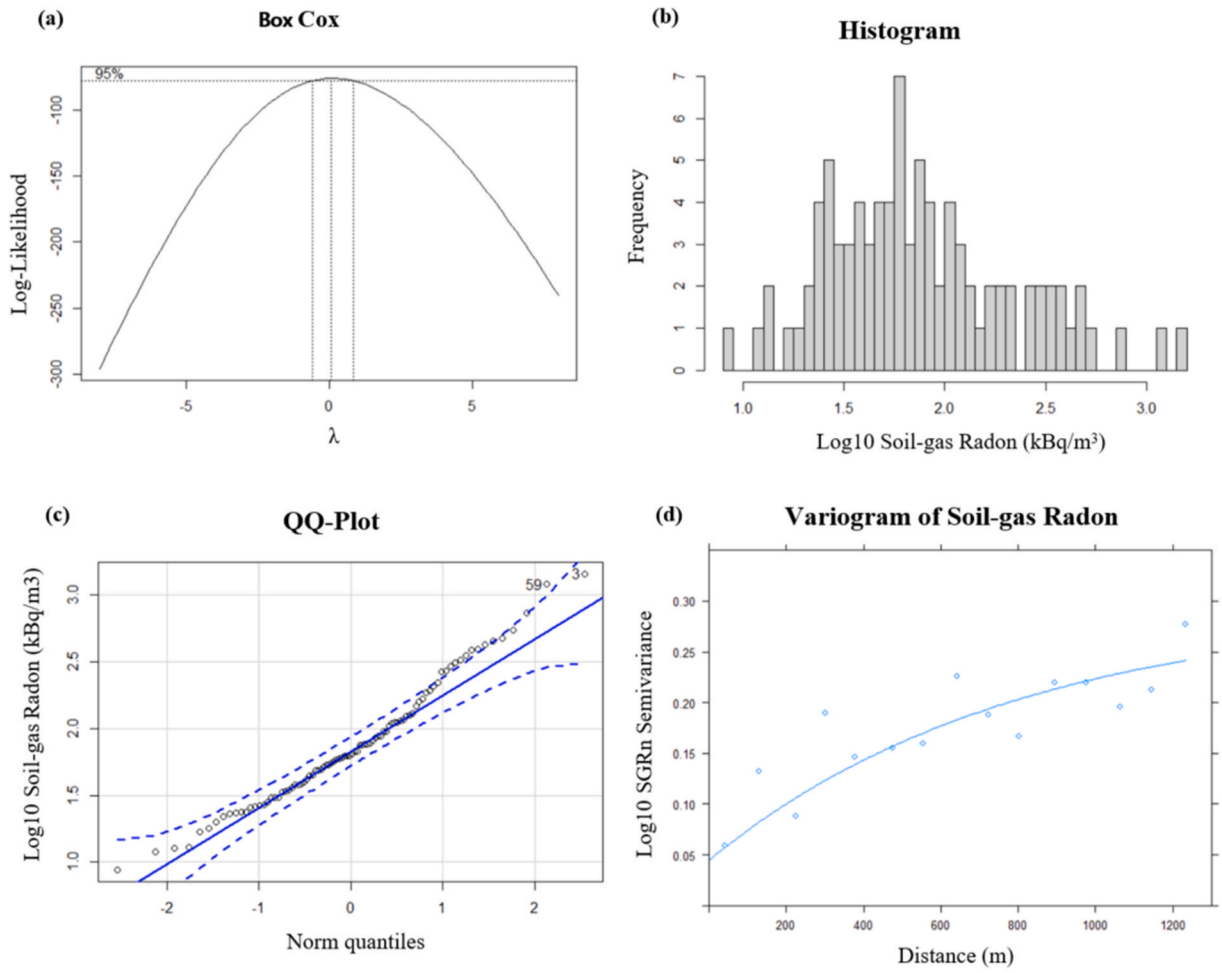

Fig. 3. (a) BoxCox (b) Histogram (c) QQ-Plot and (d) Variogram. The variogram (d) uses the "Exp" model with a nugget of 0.045, range of 800 m and psill of 0.25. of Log10 transformed soil-gas radon.

location (Singh et al., 2010). Additional differences in methodologies include some studies which use the maximum GRP and others use the median value (Günay et al., 2018; Kemski et al., 2001). In this study CRn and k measurements were taken at an approximate distribution every 250 m over a grid spacing, depending on subsoil depth and anthropogenic factors such as modification of soil profiles, or building developments. The GRP values derived from the in-situ measurements were interpolated using an inverse distance weighted kriging method with a resolution of 9 m in ArcGIS (Fig. 5b).

2.5. Indoor radon measurements

The Environmental Protection Agency (EPA) of Ireland provided the indoor radon measurements (IRC) under a specific data sharing agreement. The IRC measurements were collected between 1992 and 2017 by the Radiological Protection Institute of Ireland; this was accomplished by placing two CR-39 detectors in separate ground floor rooms for a period between three and twelve months (Fennell et al., 2002). Measurements taken over a period less than twelve months were seasonally adjusted to give an average final measurement for each dwelling; this is necessary as radon concentrations vary seasonally (Muntean et al., 2014; Organo and Murphy, 2007). For the specific study site, an IRC of 49,000 Bqm^{-3} was added to the EPA dataset with the coordinates obtained from a now-demolished house during the field survey. The spatial distribution of IRC measurements was corrected by 40 m south and 30 m east to align with their actual geographical location (Dardac, 2022), due to a formatting error in the original dataset as supplied by the EPA.

3. Results

3.1. SGRn measurements

SGRn measurements from the study site range from 8.8 $kBqm^{-3}$ (s1031) to >1433 $kBqm^{-3}$ (s109). The highest measured value of >1433 $kBqm^{-3}$ is higher than the certified detection limit of the RM-2 device, so represents a minimum value. One percent of values are very low (<10 $kBqm^{-3}$), 17% of values are low (10–30 $kBqm^{-3}$), 18% of values are moderate (30–50 $kBqm^{-3}$), 15% of values are high (50–70 $kBqm^{-3}$), 13% of values are very high (70–100 $kBqm^{-3}$), and 36% of values are extremely high (+100 $kBqm^{-3}$) (Supplementary materials). The dataset used for analysis was log10 transformed (Fig. 3). The variogram (Fig. 3d) shows that the spatial variation at a local scale is very high, with the variation levelling at 700 m. The variogram model has a nugget effect of 0.001. The sill is 0.175, model "Sph" and range 800 m.

The daily repeats give an estimate of the cumulative measurement uncertainties plus the natural variability in soil-gas radon over relatively short time scales (i.e. days). The instrument is estimated to have a ± 20% uncertainty range, as previously determined by the manufacturer and by Elío et al. (2019). We measured between 2% and 6.8% variation from each of our four daily repeat sites, which is accounted for by the instrument measurement uncertainty (Table 1).

From 88 SGRn samples, 28 were collected above Waulsortian limestones, 2 above Cloone Flagstones, 19 above the Rockfield limestones, 16 above Cracoean Reef member, 8 above Dirtoge limestones, and 15 above Clare Shales. The box plot (Fig. 4) illustrates that samples

Table 1
Daily repeats of SGRn measurements in two localities in 2018 and 2019.

Locality ID	Date	Replica	Rn(kBqm^{-3})	Mean (kBqm^{-3})	RSD (%)	RM-2 uncertainty (%)
60	July 14, 2018	A	408	438.4	9.6	6.8
	July 15, 2018	B	462			
	July 19, 2018	C	460			
	July 20, 2018	D	488			
	July 21, 2018	E	374			
23	July 16, 2018	A	59.8	33.7	37.2	2.0
	July 17, 2018	B	22.2			
	July 18, 2018	C	27.6			
	July 19, 2018	D	27.4			
	July 20, 2018	E	37.6			
	July 21, 2018	F	27.7			
67a	July 30, 2019	A	50.6	55.6	12.7	2.5
67b	July 31, 2019	B	60.6	112	1.3	3.5
	August 01, 2019	A	111			
	August 02, 2019	B	113			

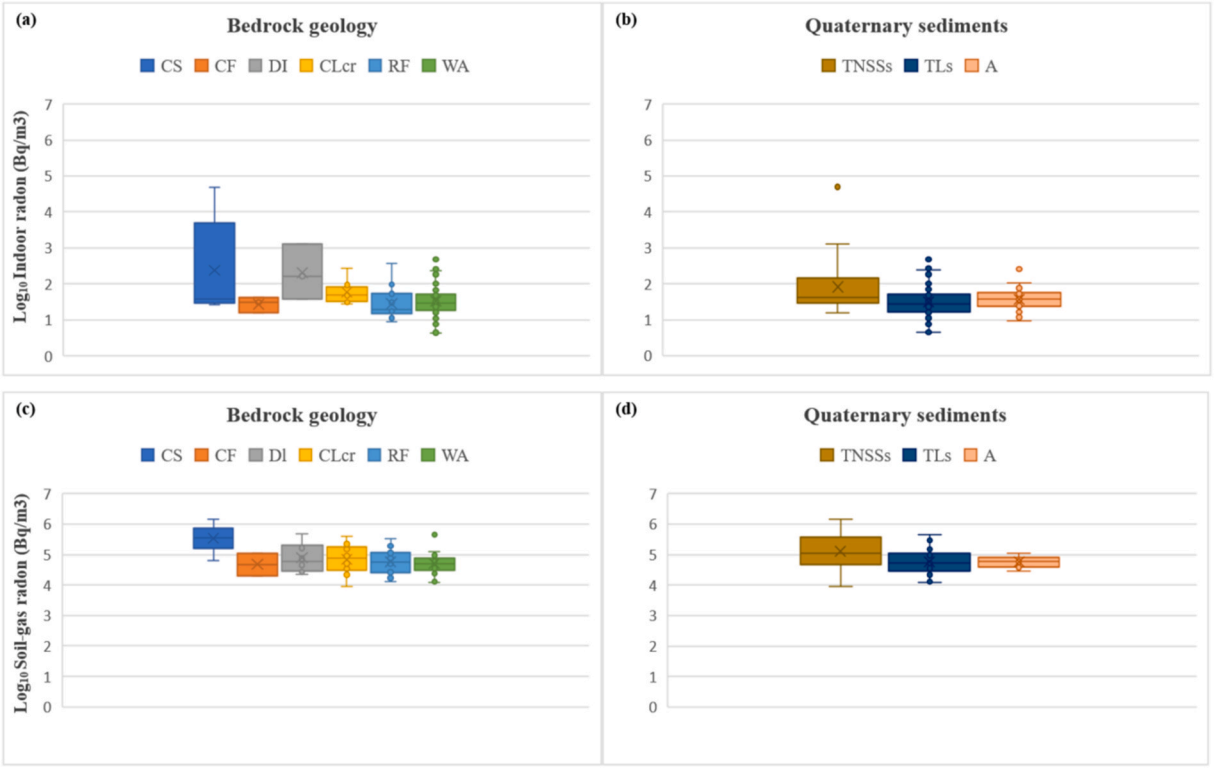

Fig. 4. Soil-gas radon results grouped to (a) bedrock geology unit. The Stratigraphic codes' full names on the plot are CS – Clare Shales, CF, Cloone Flagstones, Dl – Dirtoge limestones, CLcr – Cracoean reef member, RF – Rockfield limestone Formation, WA – Waulsortian limestones. And (b) Quaternary Sediments. The full names of the stratigraphic codes are TNSSs – Till derived from Namurian sandstones, siltstones, and shales, TLs – Till derived from limestones, A – Alluvium. Figures (c) and (d) Boxplot of Log_{10} normal Indoor radon data grouped to (c) Bedrock geology and (d) Quaternary Sediments.

collected above the Clare Shales contain higher SGRn values. The lowest values are included within the Cloone Flagstones, followed by the Waulsortian limestones, Rockfield limestones, Dirtoge limestones, and Cracoean Reef member. The majority (87%) of samples collected above the Clare Shales are exceptionally high (>100 kBqm^{-3}), whereas 86% of SGRn samples collected above the Waulsortian limestones measured below 100 kBqm^{-3} (Supplementary data file).

Analysis of variance (ANOVA) is a method used to statistically analyse the similarity of data groups based on the variance between their means (Larson, 2008). The application of ANOVA in geogenic studies is commonly used (Domingos et al., 2020; Drolet et al., 2014; Tositti et al., 2017). For the present study, one-way ANOVA is used to determine the general variance that geological factors cause in relation to SGRn. The ANOVA is repeated in a similar manner to determine the degree of IRC variation caused by geological factors, which is reported further in the results section below. The results of an ANOVA analysis statistically demonstrate a significant effect size variance of SGRn due to Quaternary geology and bedrock geology (Table 2).

Considering the Quaternary geology, 42 of the samples were collected above till derived from limestone, 37 above till derived from Namurian sandstones, siltstones, and shales, and nine were collected above alluvium (supplementary materials). The samples collected above till derived from Namurian sandstones, siltstones, and shales are mostly (59%) extremely high values. In contrast, 38% of samples collected above the till derived from limestones are greater than 100 kBqm^{-3}. All of the extremely high (>100 kBqm^{-3}) SGRn values result in a high GRP (35+), although not all of the high GRP values are linked to extremely high SGRn concentrations.

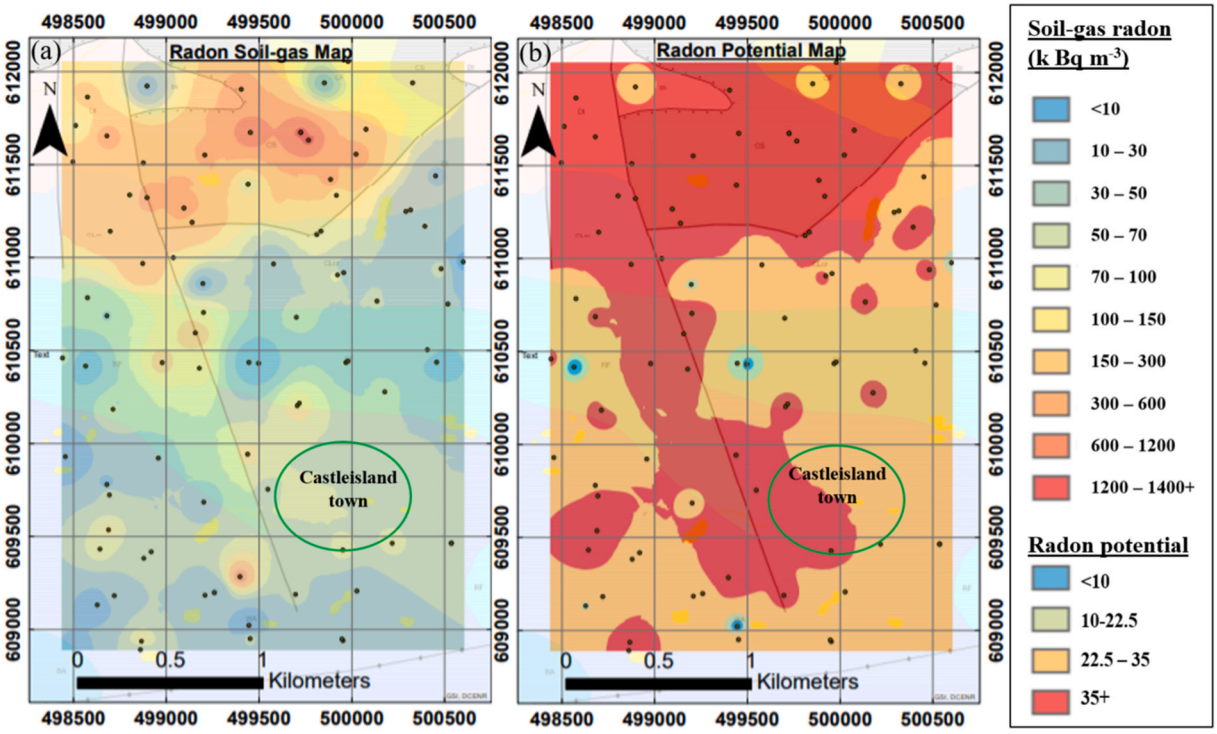

Fig. 5. (a) Soil-gas radon map and (b) radon potential map produced using Inverse distance weighted function in ArcGIS. The resulting maps have been superimposed on top of the bedrock geology 1:100 k G.S.I. map for the area. Points on the map signify where samples were collected.

Table 2
ANOVA table of soil-gas radon effect size due to subsoil permeability, Bedrock geology, and Quaternary geology. The Asterix symbols refer to the level of significance of the results. * equivalent to a p-value of 0.01, ** equivalent to a p-value of 0.001 and *** equivalent to a p-value of <0.001.

Factor	Df	Sum Sq.	Mean Sq.	F value	Pr (>F)
Subsoil permeability: variance explained 21%	4	4.327	1.082	5.578	0.000501***
Residuals	83	16.096	0.194		
Bedrock geology: variance explained 39%	5	7.728	1.546	9.983	1.74e-07 ***
Residuals	82	12.695	0.155		
Quaternary Sediments: Variance explained 13%	2	2.642	1.321	6.315	0.00726 **
Residuals	85	17.780	0.209		

Examining SGRn measurements in relation to bedrock geology (Fig. 5a) indicates higher concentrations above the Clare Shales in the north of the study area, with lower values generally above the limestones in the south of the study area. The map (Fig. 5a) reveals that higher SGRn concentrations occur above the limestones along a local NW-SE fault. Overall, 74% of the study area SGRn ranges from 8.8 k Bq m^{-3} to 100 $kBqm^{-3}$, with the most significant area (57%) equating to a moderate to high SGRn range (30 $kBqm^{-3}$ – 70 $kBqm^{-3}$). Approximately 36% of the study area contains extremely high (100+ $kBqm^{-3}$) SGRn values.

3.2. Geogenic radon potential mapping

The GRP for the study area ranges from 5 to greater than 1200. Radon Potential values greater than 35 are considered exceptionally high (Neznal et al., 2004). The resulting map (Fig. 5b) shows 49% of the area has an GRP greater than 35, 50% is medium-high, with only 1% of the site being less than 10. The north of the study area featuring Clare Shales has a GRP ranging from 200 to a maximum value of 1778, while the lowest radon potential values occur over the Rockfield Limestones Formation with a minimum value of 5.

3.3. Indoor radon

IRC values within the study area range from 4.4 Bqm^{-3} to 49,000 Bqm^{-3}. Table 3 shows that the amount of variance explained by geogenic factors using one-way ANOVA tests are 34% (16% by SGRn, 10% by bedrock geology, 4% by subsoil permeability, and 4% by Quaternary geology).

The IRC variogram (Fig. 6d) shows that the IRC measurements exhibit a relatively small degree of variation within a small spatial range (from approximately 100 m–700 m). The IRC values exhibit an increase in variation when the distance between the measurements is increased; this is reflected by the steep incline seen at approximately 800 m–1000 m on the variogram.

Table 3
ANOVA table showing the variance of Indoor Radon measurements due to Bedrock geology, Quaternary geology, soil-gas radon, and subsoil permeability. The Asterix symbols refer to the level of significance of the results. * equivalent to a p-value of 0.01, ** equivalent to a p-value of 0.001 and *** equivalent to a p-value of <0.001.

Factor	Df	Sum Sq.	Mean Sq.	F value	Pr (>F)
Bedrock geology: variance explained 10%	**7**	3.202	0.457	2.779	0.00921**
Residuals	**172**	28.315	0.165		
Quaternary geology: variance explained 4%	**2**	1.222	0.611	3.571	0.0302*
Residuals	**177**	30.295	0.171		
Soil-gas radon: variance explained 16%	**5**	5.009	1.002	6.576	1.25e-05 ***
Residuals	**174**	26.508	0.152		
Subsoil permeability: Variance explained 4%	**4**	1.361	0.340	1.974	0.1
Residuals	**175**	30.157	0.172		

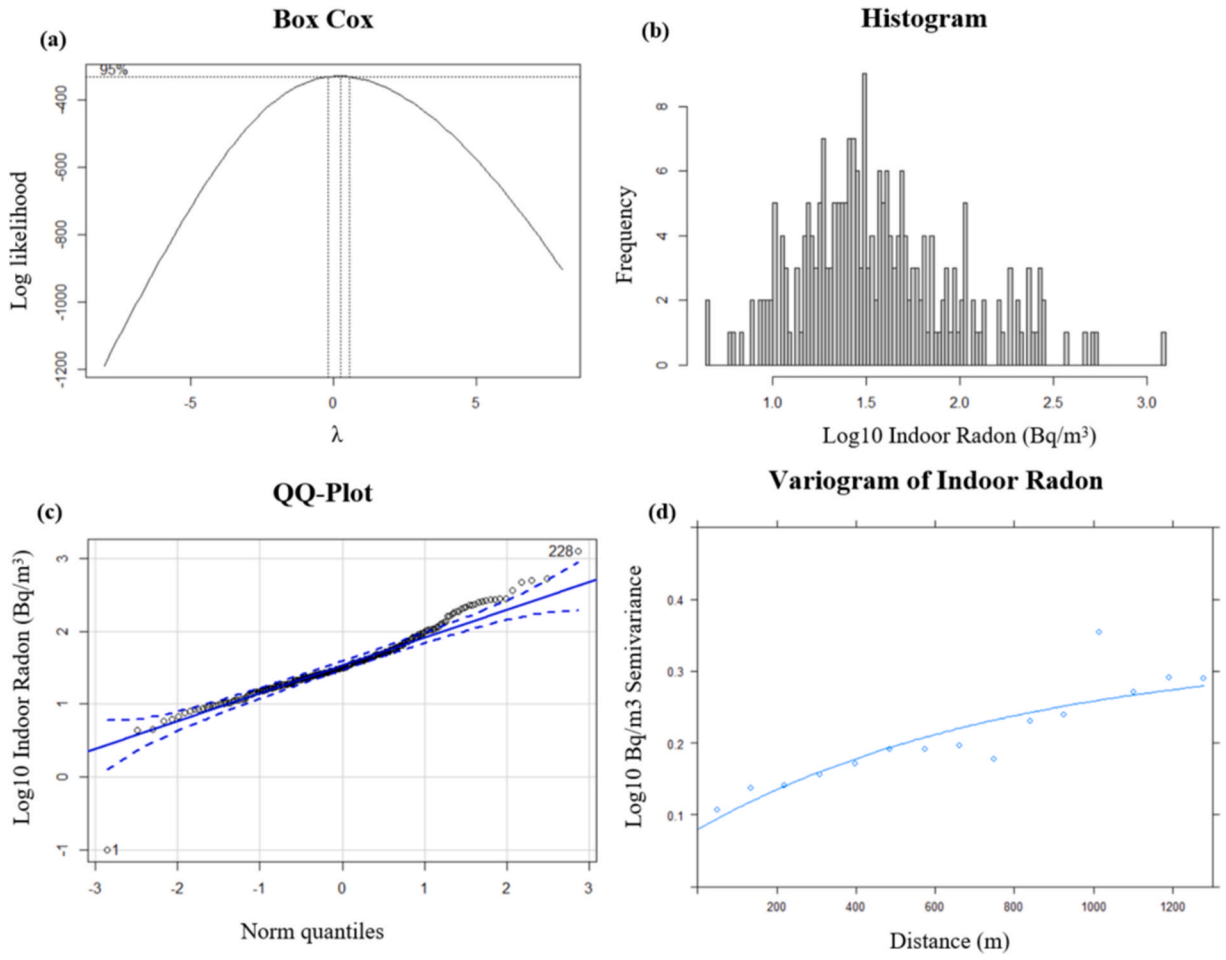

Fig. 6. Indoor radon log10 transformed data distribution. (a) BoxCox (b) Histogram (c) QQ-Plot and (d) Variogram. The variogram (d) uses the "Exp" model with a nugget of 0.08, range of 800 m and psill of 0.25.

3.3.1. Geogenic context of indoor radon results

A total of 180 houses were sampled in the area. Specifically, 144, 18, 8, 3, 4, and 3 indoor radon measurements were collected above several different bedrock lithologies (Waulsortian limestones, Rockfield limestones, Cracoean Reef member, Dirtoge limestones, Clare Shales, Cloone Flagstones, respectively) (table 6 supplementary materials). Fifteen houses (8%) have radon levels above the reference level. The probability of exceeding the reference level (table 6 supplementary material) is 8% (11 of 144 houses) for the Waulsortian limestones, 6% (1 of 18 houses) for Rockfield limestones, 12% (1 of 8 houses) for the Cracoean Reef member, 33% (1 of 3 houses) for the Dirtoge limestones, 25% (1 of 4 houses) for the Clare Shales and 0% (0 of 3 houses) for the Cloone Flagstones.

4. Discussion

Indoor radon concentrations from the study area in Castleisland, SW Ireland are amongst the highest recorded within Europe (Organo and Murphy, 2007), and are in the upper range of those recorded globally (World Health Organization, 2007). The SGRn, as might be expected from this context, are also high compared to the published literature. The median SGRn in Castleisland is ca. 66 kBqm^{-3} compared to ranges typically between ca. 10–40 kBqm^{-3} from other countries (Giustini et al., 2019; Kikaj et al., 2016; Mitra et al., 2021; Nuhu et al., 2021). In more detail, Table 4 summarizes SGRn concentrations which are typically associated with a range of different lithologies. Analysis of SGRn from Castleisland indicates that 36% of the measured samples are greater than 100 kBqm^{-3}, compared to ca. 10% of samples from other representative studies (Elío et al., 2019; Haruna et al., 2020; O'Brien et al., 2011). Globally, and in general terms, very low to moderate (<10 to 70 kBqm^{-3}) SGRn values are associated with sedimentary lithologies (Fu et al., 2017; Khan et al., 2021; Kumar et al., 2014; Szabó et al., 2014). In comparison, the sedimentary lithologies in Castleisland are associated with extremely high SGRn values (with >46.7% of samples measuring >70 kBqm^{-3}). Although radon anomalies are sometimes associated with sedimentary rocks (not including placer deposits), most occurrences of SGRn anomalies (>70 to 4000 kBqm^{-3}) are associated with granites, gneiss, or uranium-bearing deposits (Esan et al., 2020; Kemski et al., 2001; Mitra et al., 2021; Pereira et al., 2010), which contrasts with the present study area.

In relation to the GRP, several studies categorize 41% or less of an area/dataset as being in a high class (Elío et al., 2019; Giustini et al., 2019; Nuhu et al., 2021) which is lower than the 49% area (64% of samples) classified as high in this present study. The GRP in Castleisland reaches a maximum value of 1778, which is considerably higher than the limit of 35 which is conventionally considered to be high (Neznal et al., 2004). For comparison with other countries, "extreme" GRP values of ca. 40–280 have been reported elsewhere (Ciotoli et al., 2017; Pásztor et al., 2016; Szabó et al., 2014).

The original radon map of Ireland (Fig. 1) (Fennell et al., 2002) classifies the east, and south-east, of the study region as having high radon priority (with between 10% and 20% of houses above the reference level); this is in agreement with the GRP mapping carried out in this study. The NW and SW of the survey site are deemed as a high radon priority on the EPA map. The GRP (Fig. 5b) for the same sites is moderate to high with certain zones having a very high GRP. Although the

Table 4
Summary of SGRn ranges associated with lithologies in selected regions globally.

Region	Main lithologies in region	Range ($kBqm^{-3}$)	Reference
Perak state, Malaysia	Clays, granites	0.11 to 434.5	Nuhu et al. (2021)
Celleno municipality, Italy	Potassic lavas, travertine, clay-sandy clay, tuff-tuffite	6.4 to 253	Giustini et al. (2019)
Osun state, Nigeria	Gneisses and schists	0.04 to 190	Esan et al. (2020)
West Bengal, India	Granites and Gneisses	2.13 to 786	Mitra et al. (2021)
Iberian uranium province, Portugal	Granites, metasedimentary schists and greywackes	5 to 12,850	Pereira et al. (2010)
Northern Taiwan	Sandstones with silt alterations, sandstones with shales alteration	6.6 to 32.2	Fu et al. (2017)
Nova Scotia, Canada	Metasandstone, slate, granite	0.8 to 154.6	O'Brien et al. (2011)
Lesser Himalayas, Pakistan	Slate, quartzite, granite, gneiss, limestone, shale	2.3–20.1	Khan et al. (2021)
Cooley Peninsula Ireland	Sandstones, shales, granites, marine shelf facies	3.5 to 112	Elío et al. (2019)
Estonia	Sand, silt, gravel of Baltic sea deposits Glaciolacustrine clay	1 to 184 24 to 1801.6	Petersell et al. (2015)
Dharamshala, India	Sandstones	13 2 to 66.2	Kumar et al. (2014)
Central Hungary	Fluvial sand Loess (silt cemented by carbonate)	1.2 to 24.9 4.9 to 44.1	Szabó et al. (2014)

EPA radon map of Ireland and the geogenic GRP map presented here are found to be in general agreement, the GRP map has higher spatial resolution and allows for more accurate representation of areas with lower population density where IRC measurements may be lacking.

The new EPA indoor radon (Environmental Protection Agency, 2022), has higher resolution and shows greater spatial variation of radon compared to the original radon map of Ireland (Fig. 1). The higher resolution in the new radon map arises from the inclusion of four geogenic parameters (bedrock geology, Quaternary geology, aquifer type and subsoil permeability) (Elío et al., 2017; Environmental Protection Agency, 2022). The new EPA map indicates houses above the Clare Shales north of Castleisland have a low probability of exceeding the 200 Bqm^{-3} IRC reference level in Ireland (https://www.epa.ie/environment-and-you/radon/). In contrast, the SGRn and GRP maps developed in this study (Fig. 5), depict the highly anomalous SGRn (greater than 1400 $kBqm^{-3}$) and GRP (up to 1778) occurring above the Clare Shales and in the vicinity of the demolished house which measured an average IRC of 49,000 Bqm^{-3}.

The difference in designation of radon risk between the new EPA radon map and the maps created in this study, likely signifies the anomalous nature of the Clare Shales in Castleisland. Carboniferous shales from other parts of Ireland are not necessarily associated with such elevated SGRn and IRC values. In this respect, our study demonstrates that small-scale studies are useful to examine local exceptions to national-scale models.

ANOVA tests illustrate that bedrock geology explains the highest portion of the SGRn variance (39%), followed by subsoil permeability (21%) and Quaternary geology (13%) (Table 2). It is possible to estimate the variance and concentration of SGRn with reference to bedrock geology and subsoil permeability. In particular, the Clare Shales have significantly high SGRn values compared to other bedrock geology types within the study area. SGRn values from samples collected over the Carboniferous limestones display higher than generally expected from such lithologies (range 9–472 $kBqm^{-3}$, median 57 $kBqm^{-3}$) with the highest values near local faults. More elevated SGRn and subsoil permeability measurements along fault zones are commonly reported elsewhere (Miklyaev et al., 2021; Xuan et al., 2020).

The IRC results (Fig. 4a and 4b) and SGRn results share a similar trend (Fig. 4c and 4d). Noticeably, IRC data for the study area are mostly (91%) less than 200 Bqm^{-3}, aside from a few anomalous results, whereas, the SGRn results are typically (90%) between 10,000 and 350,000 Bqm^{-3}. A similar relationship between SGRn and IRC is noted by Yalım et al. (2018).

4.1. Geogenic influence on indoor radon

The influence of geogenic factors on IRC concentrations is depicted in the ANOVA table (Table 3), which shows that bedrock geology (10%) explains over twice the variance of Quaternary geology (4%), both of which are significant ($p < 0.01$); this could reflect the higher resolution/greater range of bedrock types (6) compared to Quaternary types (3).

SGRn has the most significant influence (16%) on IRC measurements. This result signifies that the greatest contributor to IRC is the radon coming from the soil-gas, which is an established concept within the literature (Åkerblom et al., 1984; Chen and Ford, 2017; World Health Organization, 2007). Since the SGRn ANOVA results (Table 2) show that bedrock geology has the most considerable influence (39%) on the SGRn concentrations, it can be argued that the bedrock geology impacts the IRC measurements indirectly by affecting the SGRn concentrations.

The combined effect of bedrock geology, Quaternary geology, SGRn and subsoil permeability for influencing indoor radon is 34% (Table 3) which compares to 30% reported for Cooley Peninsula in NE Ireland (Elío et al., 2019). Variance of indoor radon explained by bedrock geology is 10% which is in line with studies from Northern Ireland (12.1%) and SW England (10%) (Appleton et al., 2015; Ferreira et al., 2018). However, greater variance of up to 20% has been attributed to bedrock geology units in Norway, England and Wales (Appleton and Miles, 2010; Watson et al., 2017).

Considering houses with IRC above the reference level for Ireland, there is a clear difference between those located over different bedrock geology types (table 6 supplementary materials). Assigning each bedrock type an "EPA-type category" results in three units (Dirtoge limestones, Cracoean Reef member, Clare Shales) classified as high radon areas (i.e. greater than 10% of homes surpassing the reference level). The Waulsortian limestones and the Rockfield limestones would be classified as a medium radon area (between 5% and 10%). Lastly, the Cloone Flagstones would be in the lowest radon category (less than 1% of homes exceeding the reference level). Dwellings built above the Dirtoge limestones and the Clare Shales have significantly higher probability of exceeding the IRC reference level compared to other bedrock types. IRC samples which exceeded the reference level from houses built over the Dirtoge limestones were located along a fault and at the Clare Shales boundary, likely explained by their proximity to the Clare Shales and coupled with the fact that the houses are located in an area with higher radon exhalation rates due to their proximity to a fault.

Analysing the variation of IRC with reference to the Quaternary geology indicates that the till derived from Namurian siltstones, sandstones and shales contain a higher percentage of IRC exceeding the reference level (table supplementary materials). Precisely, 16% of houses located above the till derived from Namurian siltstones, sandstones and shales surpassed the reference level, compared to 9% and 3% for till derived from limestones and Alluvium, respectively. This result reinforces that geogenic information influences IRC concentrations. In particular, houses above till derived from Namurian siltstones, sandstones and shales have higher probability of exceeding the reference level.

4.2. The use of geogenic data for mapping indoor radon

Geogenic data (i.e. SGRn, bedrock and subsoil permeability) sufficiently predict the IRC categories (i.e. low, moderate, high). Bedrock

geology is the main contributor to SGRn (Table 2), whereas SGRn is most strongly associated with IRC (Table 3). As such, investigating geogenic maps of higher resolution (1:100 k) can quickly distinguish potential areas of elevated IRC. Precisely, pinpointing locations with radon source rocks and specific subsurface structures that enhance radon transportation to homes can be accomplished for regions with higher resolution geological maps which are generally publicly available. Utilizing geogenic maps for radon mapping can be extended to other bedrock units and validated by completing SGRn and subsoil permeability (i.e. GRP) surveys for representative geology types.

GRP surveys provide a substantially quicker alternative at approximately six to ten samples per day, compared to IRC surveys which requires a three-month measurement period (Elío et al., 2019; Environmental Protection Agency, 2019). GRP surveys can be especially beneficial in areas rezoned for residential use where no previous IRC measurements exist. Another benefit to using this approach is that it assesses the amount of radon available to a building regardless of the building purpose or design (workplace or home), allowing the method to be applied to mapping both the radon risk of homes as well as workplaces.

Considering that geological information is freely available online for many countries, there are several potential benefits for integrating information from existing geological maps into radon surveys. Whereas SGRn surveys are weather-dependent, there are no such constraints on utilizing existing geological map data. Indoor radon measurements are useful for constructing radon hazard maps, however the measurements themselves are prone to human error (e.g., radon detectors must be installed in specific areas of a house with limited airflow), must take place over several months, are very costly and time-consuming, or simply may not be available. Using IRC data for mapping RPAs is increasingly complex and inefficient due to tighter regulations on General Data Protection Regulations (GDPR). Field surveys which utilize existing geological maps can specifically focus on areas where an elevated radon risk is suspected, based on the geological attributes. IRC measurements could then be collected to confirm the level of IRC in each workplace or home. Furthermore, for areas where there is a lack of IRC data, it is practical to utilize the available geological data and radon-potential surveys for IRC risk mapping.

4.3. Limitations

Geogenic radon potential mapping is weather-dependent. Several days after rainfall should elapse before sampling to ensure that the soil is not water-saturated (Neznal et al., 2004). Due to weather conditions, atmospheric pressure, wind speed and temperature, SGRn varies on a daily basis (Arora et al., 2017; Kulali et al., 2017). Furthermore, SGRn varies on a seasonal basis; due to the overall mean differences in temperature and rainfall (Szabó et al., 2013). Considering these factors, it is important to ensure that soil gas samples are taken from a sufficient depth in the soil profile (usually 80–100 cm (Neznal et al., 2004)). Due to the high degree of spatial variation in SGRn concentrations, it is also important to collect several samples to obtain representative values for a given geology type, or region. Given that the original methodology of Neznal et al. (2004) has been adapted and used slightly differently in several studies, it is important to ensure different methodologies are taken into account when comparing GRP or RP from different study areas.

5. Conclusion

An approach to mapping radon-prone areas was investigated by collecting 135 soil-gas radon (SGRn) and subsoil permeability measurements across approximately 50 locations in a 6 km^2 region around Castleisland in Co. Kerry, SW Ireland. The area was chosen due to the extremely high indoor radon concentrations (average reading of 49,000 Bqm^{-3} from several measurements) previously reported from the region (Organo et al., 2004), and due to the fact that there was not a clear understanding of the source of such high values. The indoor radon concentration (IRC) variance explained by geogenic factors (bedrock geology, Quaternary geology, subsoil permeability, and SGRn) is 34%; with SGRn as the main contributor (16%). ANOVA tests illustrate that bedrock geology has the most substantial influence on SGRn concentrations (39%), although subsoil permeability (21%) and Quaternary geology (13%) also have significant effects. Results demonstrate that spatially restricted black shales, locally known as the Clare Shales, are spatially associated with both SGRn and IRC anomalies, and likely act as a radon source which may also be transported via enhanced permeability in non-mineralised fault zones and extensive subterranean karst systems which are prevalent in the region.

Geological factors (especially SGRn, bedrock geology, and subsoil permeability) sufficiently predict the IRC categories (i.e. low, moderate, high). Therefore, investigating the spatial variation and distribution of geological units in a given region can help to identify radon priority areas, particularly if reliable high-resolution maps are available, relevant radon-related data (e.g. soil properties) exist and lithologies are assigned with accuracy regarding their potential for being a point source of radon. Such an approach could pinpoint high radon areas in a very cost-efficient and time-efficient manner. The radon priority area category assigned using geological attributes can be confirmed by carrying out a geogenic radon potential survey for smaller representative areas, such as that presented in this study. Geogenic radon potential mapping can verify if an area is susceptible to high IRC. Such an approach is especially useful for areas where population density is low, and where few IRC measurements already exist. The methodology presented in this study highlights the use of combined experimental and theoretical approaches in the study of radon as a natural hazard. The approach used in this study integrates both relevant field data and geostatistical modelling, and is demonstrated to be beneficial in efforts to predict radon anomalies. Such an approach ultimately leads to a better understanding of radon in both the natural and built environments. Radon potential or hazard maps constructed using this methodology add considerable value to existing legacy geological datasets. This research also highlights the importance of reliable digital geoscience data applied to environmental exposure, and when utilized to protect the general public from the harmful effects of ionizing radiation.

Role of the funding source

The funding source (SUSI) for Méabh Banríon's Ph.D. had no involvement or role in the study design, the collection, analysis and interpretation of data; in writing of the report; and in the decision to submit the article for publication.

Declaration of competing interest

The authors declare that they have no known competing financial interests or personal relationships that could have appeared to influence the work reported in this paper.

Acknowledgements

We would like to thank the EPA for providing the InRn dataset, Ryan O'Toole, Patricia McGuire, and Winifred Duncan for part-taking in the soil-gas radon and soil permeability measurement surveys. Méabh H. Banríon would like to thank Student Universal Support Ireland (SUSI) for helping to fund their Ph.D.

Appendix A. Supplementary data

Supplementary data to this article can be found online at https://doi.org/10.1016/j.jenvrad.2022.106956.

References

Abdalla, A.M., Ismail, A.M., Al Madiy, A.A., 2021. Soil radon detection using active scintillation cell. J. Radiat. Res. Appl. Sci. 14, 16–22. https://doi.org/10.1080/16878507.2020.1783631.

Åkerblom, G., Andersson, P., Clevensjö, B., 1984. Soil gas radon - a source for indoor radon daughters. Radiat. Protect. Dosim. 7, 49–54. https://doi.org/10.1093/oxfordjournals.rpd.a082961.

Alonso, H., Rubiano, J.G., Guerra, J.G., Arnedo, M.A., Tejera, A., Martel, P., 2019. Assessment of radon risk areas in the Eastern Canary Islands using soil radon gas concentration and gas permeability of soils. Sci. Total Environ. 664, 449–460. https://doi.org/10.1016/j.scitotenv.2019.01.411.

Anderson, R.T., Vrionis, H.A., Ortiz-Bernad, I., Resch, C.T., Long, P.E., Dayvault, R., Karp, K., Marutzky, S., Metzler, D.R., Peacock, A., White, D.C., Lowe, M., Lovley, D. R., 2003. Stimulating the in situ activity of geobacter species to remove uranium from the groundwater of a uranium-contaminated aquifer. Appl. Environ. Microbiol. 69, 5884–5891. https://doi.org/10.1128/AEM.69.10.5884-5891.2003.

Appleton, J.D., Daraktchieva, Z., Young, M.E., 2015. Geological controls on radon potential in Northern Ireland. PGA (Proc. Geol. Assoc.) 126, 328–345. https://doi.org/10.1016/j.pgeola.2014.07.001.

Appleton, J.D., Miles, J.C.H., 2010. A statistical evaluation of the geogenic controls on indoor radon concentrations and radon risk. J. Environ. Radioact. 101, 799–803. https://doi.org/10.1016/j.jenvrad.2009.06.002.

Arora, B.R., Kumar, A., Walia, V., Yang, T.F., Fu, C.-C., Liu, T.-K., Wen, K.-L., Chen, C.-H., 2017. Assesment of the response of the meteorological/hydrological parameters on the soil gas radon emission at Hsinchu, northern Taiwan: a prerequisite to identify earthquake precursors. J. Asian Earth Sci. 149, 49–63. https://doi.org/10.1016/j.jseaes.2017.06.033.

Barros, N., Field, D.W., Steck, D.J., Field, R.W., 2015. Comparative survey of outdoor, residential and workplace radon concentrations. Radiat. Protect. Dosim. 163, 325–332. https://doi.org/10.1093/rpd/ncu185.

Bossew, P., 2018. Radon priority areas - definition, estimation and uncertainty. Nucl. Technol. Radiat. Protect. 33 https://doi.org/10.2298/NTRP180515011B, 11–11.

Bossew, P., Cinelli, G., Ciotoli, G., Crowley, Q., Cort, M., Elío, J., Gruber, V., Petermann, E., Tollefsen, T., 2020. Development of a geogenic radon hazard index—concept, history, experiences. Int. J. Environ. Res. Publ. Health 17, 4134. https://doi.org/10.3390/ijerph17114134.

Chen, J., Ford, K.L., 2017. A study on the correlation between soil radon potential and average indoor radon potential in Canadian cities. J. Environ. Radioact. 166, 152–156. https://doi.org/10.1016/j.jenvrad.2016.01.018.

Ciotoli, G., Voltaggio, M., Tuccimei, P., Soligo, M., Pasculli, A., Beaubien, S.E., Bigi, S., 2017. Geographically weighted regression and geostatistical techniques to construct the geogenic radon potential map of the Lazio region: a methodological proposal for the European Atlas of Natural Radiation. J. Environ. Radioact. 166, 355–375. https://doi.org/10.1016/j.jenvrad.2016.05.010.

Cucoş Dinu, A., Călugăr, M.I., Burghele, B.D., Dumitru, O.A., Cosma, C., Onac, B.P., 2017. Radon levels in Romanian caves: an occupational exposure survey. Environ. Geochem. Health 39, 1085–1099. https://doi.org/10.1007/s10653-016-9878-1.

Dardac, M., 2022. Determining the Geogenic Influence for High Indoor Radon Areas in Ireland (submitted for publication).

Domingos, F., Cinelli, G., Neves, L., Pereira, A., Braga, R., Bossew, P., Tollefsen, T., 2020. Validation of a database of mean uranium, thorium and potassium concentrations in rock samples of Portuguese geological units, generated of literature data. J. Environ. Radioact. 222, 106338 https://doi.org/10.1016/j.jenvrad.2020.106338.

Drolet, J.-P., Martel, R., Poulin, P., Dessau, J.-C., 2014. Methodology developed to make the Quebec indoor radon potential map. Sci. Total Environ. 473–474, 372–380. https://doi.org/10.1016/j.scitotenv.2013.12.039.

Duffy, J.T., Madden, J.S., Mackin, G.M., McGarry, A.T., Colgan, P.A., 1996. A reconnaissance survey of radon in show caves in Ireland. Environ. Int. 22, 415–423. https://doi.org/10.1016/S0160-4120(96)00140-7.

Duggal, V., Rani, A., Mehra, R., 2014. Measurement of soil-gas radon in some areas of northern Rajasthan, India. J. Earth Syst. Sci. 123, 1241–1247.

Elío, J., Crowley, Q., Scanlon, R., Hodgson, J., Long, S., 2019. Rapid radon potential classification using SGRn measurements in the Cooley Peninsula, County Louth, Ireland. Environ. Earth Sci. 78, 359. https://doi.org/10.1007/s12665-019-8339-4.

Elío, J., Crowley, Q., Scanlon, R., Hodgson, J., Zgaga, L., 2018. Estimation of residential radon exposure and definition of Radon Priority Areas based on expected lung cancer incidence. Environ. Int. 114, 69–76. https://doi.org/10.1016/j.envint.2018.02.025.

Elío, Javier, Crowley, Q., Scanlon, R., Hodgson, J., Long, S., 2017. Logistic regression model for detecting radon prone areas in Ireland. Sci. Total Environ. 599–600. https://doi.org/10.1016/j.scitotenv.2017.05.071.

Environmental Protection Agency, 2022. New EPA Radon maps show more homes and workplaces at risk from cancer-causing gas. https://www.epa.ie/news-releases.

Environmental Protection Agency, 2019. EPA Protocol for the Measurement of Radon in Homes and Workplaces.

Esan, D.T., Sridhar, M.K.C., Obed, R., Ajiboye, Y., Afolabi, O., Olubodun, B., Oni, O.M., 2020. Determination of residential soil gas radon risk indices over the lithological units of a southwestern Nigeria university. Sci. Rep. 10, 1–10.

European Commission, 2013. Council directive 2013/59/Euratom. Off. J. Eur. Union 2013/59/EURATOM 6–50.

Fennell, S.G., Mackin, G.M., McGarry, A.T., Pollard, D., 2002, February. Radon exposure in Ireland. Int. Congr. 1225, 71–77.

Ferreira, A., Daraktchieva, Z., Beamish, D., Kirkwood, C., Lister, T.R., Cave, M., Wragg, J., Lee, K., 2018. Indoor radon measurements in south west England explained by topsoil and stream sediment geochemistry, airborne gamma-ray spectroscopy and geology. J. Environ. Radioact. 181, 152–171. https://doi.org/10.1016/j.jenvrad.2016.05.007.

Fu, C.-C., Yang, T.F., Chen, C.-H., Lee, L.-C., Wu, Y.-M., Liu, T.-K., Walia, V., Kumar, A., Lai, T.-H., 2017. Spatial and temporal anomalies of soil gas in northern Taiwan and its tectonic and seismic implications. J. Asian Earth Sci. 149, 64–77. https://doi.org/10.1016/j.jseaes.2017.02.032.

Fuente, M., Long, S., Fenton, D., Hung, L.C., Goggins, J., Foley, M., 2020. Review of recent radon research in Ireland, OPTI-SDS project and its impact on the National Radon Control Strategy. Appl. Radiat. Isot. 163, 109210 https://doi.org/10.1016/j.apradiso.2020.109210.

Gadd, G.M., 2010. Metals, minerals and microbes: geomicrobiology and bioremediation. Microbiology 156, 609–643.

Gaskin, J., Coyle, D., Whyte, J., Krewksi, D., 2018. Global estimate of lung cancer mortality attributable to residential radon. Environ. Health Perspect. 126, 57009. https://doi.org/10.1289/EHP2503.

Giustini, F., Ciotoli, G., Rinaldini, A., Ruggiero, L., Voltaggio, M., 2019. Mapping the geogenic radon potential and radon risk by using Empirical Bayesian Kriging regression: a case study from a volcanic area of central Italy. Sci. Total Environ. 661, 449–464.

Günay, O., Saç, M.M., İçhedef, M., Taşköprü, C., 2018. Soil gas radon concentrations along the Ganos Fault (GF). Arabian J. Geosci. 11, 213. https://doi.org/10.1007/s12517-018-3542-2.

Gunn, J., 1982. Crag Cave, County Kerry, vol. 20. Irish Naturalists Journal Ltd, pp. 445–449.

Gunning, G.A., 2016. Studies of Radon in Ireland: Outdoor Levels, Detector Intercomparison and School Remediation Methods. School of Physics, Trinity College (Dublin, Ireland).

Habib, R.R., Nuwayhid, R.Y., Hamdan, Z., Alameddine, I., Katul, G., 2018. Indoor and outdoor radon concentration levels in Lebanon. Health Phys. 115.

Haruna, R., Saleh, M.A., Hashim, S., Hamzah, K., Zainal, J., Sanusi, M.S.M., 2020. Assessment of geogenic radon potential in Johor Malaysia. J. Radioanal. Nucl. Chem. 326, 1065–1074. https://doi.org/10.1007/s10967-020-07396-y.

Hodson, F., 1954. The Carboniferous rocks of Foynes island, county Limerick. Geol. Mag. 91, 153–160.

Hyun, S.P., Davis, J.A., Hayes, K.F., 2014. Abiotic U (VI) reduction by aqueous sulfide. Appl. Geochem. 50, 7–15.

Idriss, H., Salih, I., Alaamer, A.S., Abdelgalil, M., Salih, S.A., Hasan, A.M., ELtahir, M.A., Ahamed, M.M., 2014. Study of radon in soil gas, trace elements and climatic parameters around South Kordofan state, Sudan. Environ. Earth Sci. 72, 335–339.

Jelle, B.P., 2012. Development of a model for radon concentration in indoor air. Sci. Total Environ. 416, 343–350. https://doi.org/10.1016/j.scitotenv.2011.11.052.

Kemski, J., Siehl, A., Stegemann, R., Valdivia-Manchego, M., 2001. Mapping the geogenic radon potential in Germany. Sci. Total Environ. 272, 217–230. https://doi.org/10.1016/S0048-9697(01)00696-9.

Kemski, J., Klingel, R., Siehl, A., 1996. Classification and mapping of radon-affected areas in Germany. Environ. Int. 22, 789–798.

Khan, S.M., Gomes, J., Krewski, D.R., 2019. Radon interventions around the globe: a systematic review. Heliyon 5, e01737. https://doi.org/10.1016/j.heliyon.2019.e0173.

Khan, F., Khattak, S.A., Wazir, Z., Waqas, M., 2021. Spatial distribution of radon concentrations in balakot-bagh (B–B) fault line and adjoining areas, lesser himalayas, north Pakistan. Environ. Earth Sci. 80, 291. https://doi.org/10.1007/s12665-021-09569-8.

Kikaj, D., Jeran, Z., Bahtijari, M., Stegnar, P., 2016. Radon in soil gas in Kosovo. J. Environ. Radioact. 164, 245–252. https://doi.org/10.1016/j.jenvrad.2016.07.037.

Koribanics, N.M., Tuorto, S.J., Lopez-Chiaffarelli, N., McGuinness, L.R., Häggblom, M. M., Williams, K.H., Long, P.E., Kerkhof, L.J., 2015. Spatial distribution of an uranium-respiring betaproteobacterium at the rifle, CO field research site. PLoS One 10, e0123378. https://doi.org/10.1371/journal.pone.0123378.

Kulali, F., Akkurt, I., Özgür, N., 2017. The effect of meteorological parameters on radon concentration in soil gas. Acta Phys. Pol., A 132, 999–1001.

Kumar, A., Arora, V., Walia, V., Bajwa, B.S., Singh, S., Yang, T.F., 2014. Study of soil gas radon variations in the tectonically active Dharamshala and Chamba regions, Himachal Pradesh, India. Environ. Earth Sci. 72, 2837–2847.

Laiolo, M., Ranaldi, M., Tarchini, L., Carapezza, M.L., Coppola, D., Ricci, T., Cigolini, C., 2016. The effects of environmental parameters on diffuse degassing at Stromboli volcano: insights from joint monitoring of soil CO2 flux and radon activity. J. Volcanol. Geoth. Res. 315, 65–78. https://doi.org/10.1016/j.jvolgeores.2016.02.004 0377-0273.

Larson, M.G., 2008. Analysis of variance. Circulation 117, 115–121. https://doi.org/10.1161/CIRCULATIONAHA.107.654335.

Lecomte, A., Cathelineau, M., Michels, R., Peiffert, C., Brouand, M., 2017. Uranium mineralization in the Alum Shale Formation (Sweden): evolution of a U-rich marine black shale from sedimentation to metamorphism. Ore Geol. Rev. 88, 71–98. https://doi.org/10.1016/j.oregeorev.2017.04.021.

Liping, H.E., Chen, B., Zhao, C., Zhuo, W., 2016. The study on effects of indoor air filtration on radon exposure to residents. Chin. J. Radiol. Med. Protect. 36, 688–693.

Margineanu, R.M., 2019. Radon measurements in underground mines and caves from several European countries. In: AIP Conference Proceedings. AIP Publishing LLC, p. 50004.

Marsh, J.W., Tomášek, L., Laurier, D., Harrison, J.D., 2021. Effective dose coefficients for radon and progeny: a review of ICRP and UNSCEAR values. Radiat. Protect. Dosim. 195, 1–20. https://doi.org/10.1093/rpd/ncab106.

Miklyaev, P.S., Petrova, T.B., Shchitov, D.V., Sidyakin, P.A., Murzabekov, M.A., Marennyy, A.M., Nefedov, N.A., Sapozhnikov, Y.A., 2021. The results of long-term

simultaneous measurements of radon exhalation rate, radon concentrations in soil gas and groundwater in the fault zone. Appl. Radiat. Isot. 167, 109460 https://doi.org/10.1016/j.apradiso.2020.109460.
Min, M., Xu, H., Fayek, Mostafa, Chen, J., 2005. Evidence of uranium biomineralization in sandstone-hosted roll-front uranium deposits, northwestern China. Ore Geol. Rev. 26 https://doi.org/10.1016/j.oregeorev.2004.10.003.
Mitra, S., Chowdhury, S., Mukherjee, J., Sutradhar, S., Mondal, S., Barman, C., Deb, A., 2021. Assessment of radon (222Rn) activity in groundwater and soil-gas in Purulia district, West Bengal, India. J. Radioanal. Nucl. Chem. 330, 1331–1338.
Monty, C., 2000. UNSCEAR report 2000: sources and effects of ionizing radiation. J. Radiol. Prot. 21 https://doi.org/10.1088/0952-4746/21/1/609.
Muntean, L.E., Cosma, C., Cucos, A., Dicu, T., Moldovan, D.V., 2014. Assessment of annual and seasonal variation of indoor radon levels in dwelling houses from Alba County, Romania. Rom. J. Phys. 59, 163–171.
Murphy, Dowdall, Long, Curtin, Fenton, 2021. Estimating population lung cancer risk from radon using a resource efficient stratified population weighted sample survey protocol–Lessons and results from Ireland. J. Environ. Radioact. 233 https://doi.org/10.1016/j.jenvrad.2021.106582.
Nagarajan, R., Madhavaraju, J., Nagendra, R., Armstrong-Altrin, J.S., Moutte, J., 2007. Geochemistry of neoproterozoic shales of the rabanpalli formation, bhima basin, northern Karnataka, southern India: implications for provenance and paleoredox conditions. Rev. Mex. Ciencias Geol. 24, 150–160.
National Cancer Registry Ireland, 2020. Cancer in Ireland 1994-2018 with Estimates for 2018-2020: Annual Report of the National Cancer Registry.
National Radon Control Strategy, 2019. NRCS Knowledge Gaps Phase 2.
Neznal, Matěj, Neznal, Martin, Matolin, M., Barnet, I., Miksova, J., 2004. The New Method for Assessing the Radon Risk of Building Sites. Czech Geological Survey Prague.
Nuhu, H., Hashim, S., Aziz Saleh, M., Syazwan Mohd Sanusi, M., Hussein Alomari, A., Jamal, M.H., Abdullah, R.A., Hassan, S.A., 2021. Soil gas radon and soil permeability assessment: mapping radon risk areas in Perak State, Malaysia. PLoS One 16, e0254099.
O'Brien, K., Goodwin, T., Risk, D., 2011. Radon soil gas in the halifax regional municipality, nova scotia, Canada. Atl. Geol. 47, 112–124.
Organo, C., Ellard, A., Fenton, D., Synnott, H., O'Colmáin, M., Prenter, S., O'Reilly, S., Colgan, P., 2004. High radon concentrations in a house near Castleisland, County Kerry (Ireland)—identification, remediation and post-remediation. J. Radiol. Prot. 24, 107. https://doi.org/10.1088/0952-4746/24/2/001.
Organo, C., Murphy, P., 2007. The Castleisland Radon Survey—follow-up to the discovery of a house with extremely high radon concentrations in County Kerry (SW Ireland). J. Radiol. Prot. 27 https://doi.org/10.1088/0952-4746/27/3/002.
Pásztor, L., Szabó, K.Z., Szatmári, G., Laborczi, A., Horváth, Á., 2016. Mapping geogenic radon potential by regression kriging. Sci. Total Environ. 544, 883–891. https://doi.org/10.1016/j.scitotenv.2015.11.175.
Petermann, E., Bossew, P., Hoffmann, B., 2022. Radon hazard vs. radon risk - on the effectiveness of radon priority areas. J. Environ. Radioact. 244–245, 106833 https://doi.org/10.1016/j.jenvrad.2022.106833.
Petersell, V., Jüriado, K., Raukas, A., Shtokalenko, M., Täht-Kok, K., 2015. Quaternary deposits and weathered bedrock material as a source of dangerous radon emissions in Estonia. Geologos 21.
Pereira, A., Godinho, M., Neves, L., 2010. On the influence of faulting on small-scale soil-gas radon variability: a case study in the Iberian Uranium Province. J. Environ. Radioact. 101, 875–882.
Pracht, M., 1997. Geology of Kerry - Cork: A Geological Description to Accompany the Bedrock Geology 1:100,000 Scale Map Series, Sheet 21. Kerry-Cork.
Radiological Protection Act, 1991. (Ionising Radiation) Regulations, 2019. Statutory Instruments Ireland, S.I. No. 30 of 2019.
Rafique, M., Abbasi, S., Shahzadi, C., Basharat, M., Jabbar, A., Ur Rahman, S., 2021. Excessive lifetime cancer risk assessment due to short-term indoor/outdoor ambient radon and gamma dose rate exposures. Iran. J. Sci. Technol. Trans. A-Science 45, 2181–2190. https://doi.org/10.1007/s40995-021-01192-3.
Ravikumar, P., Davis, D., Somashekar, R., Prakash, K., 2015. Measurement of radon activity in soil gas using RAD7 in the Environs of Chitradurga District, Karnataka, India. Elixir. Earth. Sci. 80, 31078–31082.
Rider, M., 1974. The Namurian of West County Clare. Presented at the Proceedings of the Royal Irish Academy. Section B: Biological. Geological, and Chemical Science, JSTOR, pp. 125–142.
Schubert, M., Musolff, A., Weiss, H., 2018. Influences of meteorological parameters on indoor radon concentrations (222Rn) excluding the effects of forced ventilation and radon exhalation from soil and building materials. J. Environ. Radioact. 192, 81–85. https://doi.org/10.1016/j.jenvrad.2018.06.011.
Singh, J., Singh, H., Singh, S., Bajwa, B., 2010. Measurement of soil gas radon and its correlation with indoor radon around some areas of Upper Siwaliks, India. J. Radiol. Prot. 30, 63.
Sleeman, A., MacConnell, B., Gatley, S., 2004. Understanding Earth Processes, Rocks and the Geological History of Ireland: A Companion to the 1: 1.000. 000 Scale Bedrock Geological Map of Ireland. Geological Survey of Ireland.
Smith, M.E., Dumitru, O.A., Burghele, B.D., Cucoș, A., Onac, B.P., 2019. Radon concentration in three Florida caves: Florida, Jennings, and Ocala. Carbonates Evaporites 34, 433–439. https://doi.org/10.1007/s13146-018-0473-7.
Soesoo, A., Vind, J., Hade, S., 2020. Uranium and thorium resources of Estonia. Minerals 10. https://doi.org/10.3390/min10090798.
Sun, K., Guo, Q., Cheng, J.G., 2004. The effect of some soil characteristics on soil radon concentration and radon exhalation from soil surface. J. Nucl. Sci. Technol. 41 (11), 1113–1117. https://doi.org/10.1080/18811248.2004.9726337.
Sundal, A.V., Valen, V., Soldal, O., Strand, T., 2008. The influence of meteorological parameters on soil radon levels in permeable glacial sediments. Sci. Total Environ. 389, 418–428. https://doi.org/10.1016/j.scitotenv.2007.09.001.
Szabó, K.Z., Jordan, G., Horváth, Á., Szabó, C., 2014. Mapping the geogenic radon potential: methodology and spatial analysis for central Hungary. J. Environ. Radioact. 129, 107–120.
Szabó, K.Z., Jordan, G., Horváth, Á., Szabó, C., 2013. Dynamics of soil gas radon concentration in a highly permeable soil based on a long-term high temporal resolution observation series. J. Environ. Radioact. 124, 74–83. https://doi.org/10.1016/j.jenvrad.2013.04.004.
Thornton, M.S., 1966. The Lower Carboniferous Limestones of the Tralee Bay Area, Co. Kerry, Ireland. Unpublished PhD thesis, University of Cambridge.
Tooth, A., Fairchild, I., 2003. Soil and karst aquifer hydrological controls on the geochemical evolution of speleothem-forming drip waters, Crag Cave, Southwest Ireland. J. Hydrol. 273, 51–68. https://doi.org/10.1016/S0022-1694(02)00349-9.
Tositti, L., Cinelli, G., Brattich, E., Galgaro, A., Mostacci, D., Mazzoli, C., Massironi, M., Sassi, R., 2017. Assessment of lithogenic radioactivity in the Euganean Hills magmatic district (NE Italy). J. Environ. Radioact. 166, 259–269. https://doi.org/10.1016/j.jenvrad.2016.07.011.
United Nations Scientific Committee on the Effects of Atomic Radiation, 2015. Report of the United Nations Scientific Committee on the Effects of Atomic Radiation to the General Assembly.
Watson, R.J., Smethurst, M.A., Ganerød, G.V., Finne, I., Rudjord, A.L., 2017. The use of mapped geology as a predictor of radon potential in Norway. J. Environ. Radioact. 166, 341–354. https://doi.org/10.1016/j.jenvrad.2016.05.031.
Wignall, P., Best, J., 2000. The western Irish Namurian basin reassessed. Basin Res. 12, 59–78. https://doi.org/10.1046/j.1365-2117.2000.00113.x.
World Health Organization, 2009. In: WHO Handbook on Indoor Radon: a Public Health Perspective. World Health Organization.
World Health Organization, 2007. International Radon Project: Survey on Radon Guidelines, Programmes and Activities (No. World Health Organization. WHO/HSE/RAD/07.01).
Xuan, P., Duong, N., Chinh, V., Dang, P., Qua, N., Pho, N., 2020. Soil gas radon measurement for identifying active faults in thua thien hue (vietnam). J. Geosci. Environ. Protect. 8 https://doi.org/10.4236/gep.2020.87003.
Xie, D., Liao, M., Kearfott, K.J., 2015. Influence of environmental factors on indoor radon concentration levels in the basement and ground floor of a building–A case study. Radiat. Meas. 82, 52–58.
Yalım, H.A., Gümüş, A., Başaran, C., Bağcı, M., Yıldız, A., Açil, D., Özçelik, M., İlhan, M. Z., Ünal, R., 2018. Comparison of radon concentrations in soil gas and indoor environment of Afyonkarahisar Province. Arabian J. Geosci. 11, 246. https://doi.org/10.1007/s12517-018-3546-y.